REGULAR ARTICLE

blood advances

Genetic and evolutionary patterns of treatment resistance in relapsed B-cell lymphoma

Christopher K. Rushton,[1,*] Sarah E. Arthur,[1,2,*] Miguel Alcaide,[1] Matthew Cheung,[1] Aixiang Jiang,[1,2] Krysta M. Coyle,[1] Kirstie L. S. Cleary,[3] Nicole Thomas,[1] Laura K. Hilton,[1] Neil Michaud,[4] Scott Daigle,[4] Jordan Davidson,[1] Kevin Bushell,[1] Stephen Yu,[1] Ryan N. Rys,[5] Michael Jain,[6] Lois Shepherd,[7] Marco A. Marra,[8] John Kuruvilla,[9] Michael Crump,[9] Koren Mann,[10,11] Sarit Assouline,[11] Joseph M. Connors,[2] Christian Steidl,[2] Mark S. Cragg,[3] David W. Scott,[2] Nathalie A. Johnson,[5,†] and Ryan D. Morin[1,8,†]

[1]Department of Molecular Biology and Biochemistry, Simon Fraser University, Burnaby, BC, Canada; [2]Centre for Lymphoid Cancer, BC Cancer, Vancouver, BC, Canada; [3]Faculty of Medicine, University of Southampton, Southampton, United Kingdom; [4]Epizyme, Cambridge, MA; [5]McGill University, Montreal, QC, Canada; [6]Department of Blood and Marrow Transplant and Cellular Immunotherapy, Moffitt Cancer Center, Tampa, FL; [7]Canadian Cancer Trials Group, Queen's University, Kingston, ON, Canada; [8]Genome Sciences Centre, BC Cancer, Vancouver, BC, Canada; [9]Princess Margaret Cancer Centre, Toronto, ON, Canada; and [10]Lady Davis Institute for Medical Research, [11]Jewish General Hospital, Montreal, QC, Canada

Key Points

- *KMT2D* and *TP53* are predominantly mutated in rrDLBCL and remain clonally stable following therapy.
- *MS4A1* mutations are commonly acquired and undergo clonal expansion following treatment with rituximab-containing therapy.

Diffuse large B-cell lymphoma (DLBCL) patients are typically treated with immunochemotherapy containing rituximab (rituximab, cyclophosphamide, hydroxydaunorubicin-vincristine (Oncovin), and prednisone [R-CHOP]); however, prognosis is extremely poor if R-CHOP fails. To identify genetic mechanisms contributing to primary or acquired R-CHOP resistance, we performed target-panel sequencing of 135 relapsed/refractory DLBCLs (rrDLBCLs), primarily comprising circulating tumor DNA from patients on clinical trials. Comparison with a metacohort of 1670 diagnostic DLBCLs identified 6 genes significantly enriched for mutations upon relapse. *TP53* and *KMT2D* were mutated in the majority of rrDLBCLs, and these mutations remained clonally persistent throughout treatment in paired diagnostic-relapse samples, suggesting a role in primary treatment resistance. Nonsense and missense mutations affecting *MS4A1*, which encodes CD20, are exceedingly rare in diagnostic samples but show recurrent patterns of clonal expansion following rituximab-based therapy. *MS4A1* missense mutations within the transmembrane domains lead to loss of CD20 in vitro, and patient tumors harboring these mutations lacked CD20 protein expression. In a time series from a patient treated with multiple rounds of therapy, tumor heterogeneity and minor *MS4A1*-harboring subclones contributed to rapid disease recurrence, with *MS4A1* mutations as founding events for these subclones. *TP53* and *KMT2D* mutation status, in combination with other prognostic factors, may be used to identify high-risk patients prior to R-CHOP for posttreatment monitoring. Using liquid biopsies, we show the potential to identify tumors with loss of CD20 surface expression stemming from *MS4A1* mutations. Implementation of noninvasive assays to detect such features of acquired treatment resistance may allow timely transition to more effective treatment regimens.

Introduction

Diffuse large B-cell lymphoma (DLBCL) is the most common type of non-Hodgkin lymphoma, representing 30% to 40% of cases diagnosed in North America. DLBCL can arise de novo or through histologic

Submitted 18 February 2020; accepted 14 May 2020; published online 26 June 2020.
DOI 10.1182/bloodadvances.2020001696.

*C.K.R. and S.E.A. contributed equally to this work.

†N.A.J. and R.D.M. contributed equally to this work.

All liquid biopsy DNA sequencing data generated in this study have been deposited into the EGA under the following accession number: EGAS00001004469. Previous published rrDLBCL exome cases can be obtained from the EGA as described in the appropriate publication.

The full-text version of this article contains a data supplement.

transformation from indolent lymphoid malignancies, most commonly transformed follicular lymphoma (tFL). Patients diagnosed with DLBCL are generally treated with a standard immunochemotherapy regimen comprising 4 chemotherapeutic agents and the anti-CD20 monoclonal antibody (mAb) rituximab (rituximab, cyclophosphamide, hydroxydaunorubicin, vincristine [Oncovin], and prednisone [R-CHOP]), which is curative for 60% to 70% of DLBCL cases.[1,2] However, for patients with DLBCL that is refractory to frontline treatment and those who experience subsequent relapse (relapsed/refractory DLBCL or rrDLBCL), outcomes are extremely poor, with a 2-year overall survival of 20% to 40%.[3,4] Although numerous treatments are under investigation to improve both frontline and salvage therapy, the success of these new therapies has been limited. The advancement of therapeutics in the relapse setting has likely been encumbered by our limited understanding of the molecular features that underlie resistance to R-CHOP. Identifying such mechanisms may reveal additional treatment options and lead to biomarkers allowing patients to be paired with appropriate treatments.

Whereas the genomic landscape of diagnostic DLBCL is well understood, the genomic features of both rrDLBCL and DLBCLs that arise through histologic transformation remain elusive due to the difficulties in obtaining tumor tissue from relapsed patients. Early studies exploring the genetics of rrDLBCL identified several candidate genes enriched for mutations among rrDLBCL cases, including *TP53*, *STAT6*, *FOXO1*, *SOCS1*, and *PIM1*.[5-7] Indeed, mutations in some of these are prognostic at diagnosis (eg, *FOXO1*[8] and *TP53*[9,10]), whereas others may reflect a more diverse representation of DLBCLs beyond those arising de novo, including tFLs. Previous studies of rrDLBCL have been limited by small sample sizes, with the largest single cohort comprising 47 cases.[11] In addition to comparing mutation prevalence between untreated DLBCL and rrDLBCL, some studies compared the clonal population structure and mutation burden between paired diagnostic and relapse samples.[11,12] Such analyses identified additional candidate genes whose mutation could contribute to treatment resistance, such as *BCL2* and *CREBBP*,[11] but these results have not been independently confirmed. The genetic heterogeneity of DLBCL warrants a comprehensive study of rrDLBCL to definitively identify genes whose mutation may afford resistance to components of R-CHOP.

Although cell-free DNA is commonly used for noninvasive quantitative monitoring of disease burden,[13-15] with sufficient levels of circulating tumor DNA (ctDNA), liquid biopsies can also provide a source of tumor genetic material allowing broad genetic characterization of tumors.[16-18] In DLBCL, mutations found within ctDNA reflect somatic mutations irrespective of anatomical biases, providing opportunity for comprehensive exploration of tumor genetics and heterogeneity.[19] This can be accomplished using a single time point[20] but is more powerful when applied to serial samples as the variant allele frequency can reveal clonal dynamics and thus putative resistance mechanisms.[21]

To more thoroughly survey the genetic mechanisms of R-CHOP resistance in DLBCL, we explored the genetics of rrDLBCL in 135 cases relying on a combination of tumor tissue and plasma-derived ctDNA collected after relapse. By comparing the mutational profiles of these cases to a large cohort of untreated DLBCLs, we identified 6 genes significantly enriched for mutations. Many of these genes are commonly mutated in untreated DLBCL, notably *KMT2D* and *TP53*, and remain clonally stable over the course of therapy. Another of these genes, *MS4A1*, encodes the B-cell surface marker CD20 and is the target of rituximab. *MS4A1* missense mutations are restricted to transmembrane domains and inhibit binding of both rituximab and other anti-CD20 antibodies. These finding have the potential to identify patients at a high risk of R-CHOP failure prior to frontline treatment and those with tumors likely to be resistant to rituximab-based secondary therapies and other CD20-targeted immunotherapies.

Methods

Targeted sequencing and mutational analysis of rrDLBCLs

This study included samples from 135 patients with rrDLBCL with 117 of these comprising plasma collected within 3 clinical trials or the general patient population treated in Quebec (supplemental Table 1). This study was reviewed and approved by the Research Ethics Boards of the University of British Columbia-BC Cancer and the Jewish General Hospital (18-030), in accordance with the Declaration of Helsinki. Plasmas were collected and processed as previously described[18,22] and detailed in the supplemental Methods. The remaining 18 cases represent tissue biopsies previously described by our group (supplemental Table 2).[6] With the exception of these 18 cases with existing exome data, all samples were subjected to library construction using custom adaptors with unique molecule identifiers. Libraries were enriched by hybridization-capture using a custom set of LockDown oligonucleotides targeting the exons of 63 genes (supplemental Table 3). The genes on this panel represent well-established DLBCL genes from previous publications and included *MS4A1* based on preliminary exome and genome data from PT255 and the 18 rrDLBCL exomes. Following enrichment, all libraries were multiplexed and sequenced using Illumina chemistry using 125- or 150-bp paired reads on either MiSeq or HiSeq2500 instruments. After alignment, reads were collapsed into consensus sequences using in-house pipeline that leverages unique molecule identifier information. Single nucleotide variants and small insertions and deletions (henceforth simple somatic mutations) were identified with Strelka2[23] with custom postfiltration steps to remove artifacts (supplemental Methods; supplemental Table 4).

Metaanalysis of untreated DLBCLs

To obtain a cohort representative of diagnostic DLBCLs, we compiled exome data from 3 previously published cohorts[24-26] and a cohort of paired tumor/normal genomes,[27] amounting to 1670 cases termed the "untreated" cohort, because all biopsies were obtained prior to treatment. As matched constitutional samples were not available for the majority of these exome cases, and because the supplied variant calls were generated using diverse pipelines, we reprocessed all exomes through a standardized variant calling workflow for unpaired tumor samples, including filtering of common and rare germline variants (supplemental Methods; supplemental Figure 1).

Identifying genes associated with rrDLBCL

We identified mutations and hotspots associated with rrDLBCL using 2 complementary approaches. First, we compared the gene and hotspot mutation frequency between rrDLBCL and untreated DLBCL to identify genes enriched for mutations in rrDLBCL.

Mutation hotspots considered here are listed in supplemental Table 5. The mutation frequency of all genes in our panel was compared between the rrDLBCL cohort and the untreated DLBCL cohort, as well as an additional diagnostic cohort,[28] using Fisher's exact test and Benjamini and Hochberg false discovery rate threshold of <0.1 (supplemental Table 6; supplemental Table 7). Second, leveraging the paired samples representing time points prior to and following treatment (supplemental Table 8), we compared the tumor genomic landscape between time points to identify genes that recurrently showed evidence of clonal selection. Mutations were classified based on the log ratio of the cancer cell fraction (CCF) between the 2 time points, where log-fold change (T2 CCF)/(T1 CCF) > 1.0 indicates a mutation underwent clonal expansion following treatment, log-fold change < -1.0 indicated the mutation was depleted following treatment, with all other values considered stable. We also explored the prevalence of different genetic subgroups using the LymphGen classifier (supplemental Methods; supplemental Tables 2 and 9).[29]

Evaluation of *MS4A1* protein expression and antibody reactivity

Suspension-adapted Chinese hamster ovary (CHO-S) cells (Life Technologies) were cultured in FreestyleCHO media supplemented with 8 mM glutamine (Gibco). Cells were maintained between 0.3 and 1.5 $\times$ 10^6 cells/mL in a humidified shaking incubator at 37°C in 8% CO_2. CHO-S cells (10^7) were transfected with 10 μg of plasmid DNA containing *MS4A1* wild-type (WT) or mutant constructs. Details of mutagenesis are included in supplemental Methods and supplemental Table 10. For each transfection, efficiency was determined using a positive control (green fluorescent protein [GFP]) to demonstrate that cells were permissive for transfections. For all experiments, WT CD20 transfections were performed in parallel with mutants. Transfected cells (1.5 $\times$ 10^5) were opsonized with 1.5 μg of unlabeled anti-CD20 antibody for 30 minutes at 4°C. Unbound antibody was washed twice in 2 mL wash buffer (phosphate-buffered saline containing 1% bovine serum albumin and 10 mM sodium azide) and centrifuged at 400*g* for 5 minutes and resuspended in ~150 μL of wash buffer. Primary antibody was detected with 0.2 μg/mL of anti-human immunoglobulin G (IgG)–phycoerythrin or anti-mouse IgG-phycoerythrin polyclonal antibodies (Stratech) and stained for 30 minutes at 4°C. Cells were washed in 2 mL of wash buffer before acquiring on a FACSCalibur fluorescence-activated cell sorter. Flow cytometry data were analyzed in FCSExpress v.3 (De Novo software, Pasadena, CA). rituximab (human [h]IgG1), ofatumumab (hIgG1), tositumomab (B1, murine [m]IgG1), and obinutuzumab (non-glycomodified hIgG1 type II relative of obinutuzumab) or an isotype control (mIgG1 or hIgG1) were used to stain the cells. Immunoblotting was performed largely as reported previously.[30] In brief, 5 $\times$ 10^6 cells were lysed in radioimmunoprecipitation assay buffer with 20 μg separated on a 10% Bis-Tris gel. CD20 expression was assessed using rabbit anti-CD20 clone EP459Y (Abcam) alongside an HRP-conjugated anti-rabbit secondary antibody (NA9340, Sigma) detected using a ChemiDoc-It Imaging System. Full details of immunoblotting are included in supplemental Methods.

PT255 exome sequencing and single-cell analysis

We performed exome sequencing on a single relapsed case (PT255) representing 3 time points: (1) the diagnostic biopsy (diagnosis, D); (2) cell-free DNA (cfDNA) collected following second relapse (relapse 2, R2/P1); and (3) cfDNA collected following third relapse (relapse 3, R3/P5). Somatic variants, copy number alterations, and clonal population structure were analyzed as described above. Somatic coding variants were chosen from this bulk tumor and plasma exome sequencing to represent different clones at varying time points (supplemental Table 11). The Fluidigm Access Array was used for multiplexing amplicon sequencing of selected variants in PT255 plasma samples and circulating tumor single cells from selected time points following relapse (supplemental Table 12).

Results

Enrichment of mutations in rrDLBCL

The pattern of mutations observed in rrDLBCL largely resembles that of untreated DLBCL (Figure 1). As this survey was focused on the genetic landscape following relapse, we searched for genes enriched for mutations after treatment failure. Such mutations are expected to represent either features of primary treatment resistance or examples of mutations subjected to clonal expansion under the selective pressures exerted by therapy. This analysis revealed 6 genes enriched for mutations: *KMT2D*, *TP53*, *CREBBP*, *FOXO1*, *NFKBIE*, and *MS4A1*, with another 2 genes depleted for mutations in rrDLBCL (Figure 2).

The lysine methyltransferase *KMT2D* is a tumor suppressor in DLBCL and follicular lymphoma (FL)[31] and was mutated in half of all rrDLBCLs (Figure 2A). In addition to a significant increase in *KMT2D* mutations in rrDLBCL relative to untreated DLBCL (q = 0.0678; OR, 1.68), loss-of-function mutations were even more strongly enriched at relapse (55/135 rrDLBCLs [40.7%] vs 304/1314 untreated [23.1%], $q = 1.7 \times 10^{-5}$). Similar to the pattern in untreated cases, truncating mutations were observed across the length of the protein (Figure 3A) and tend to occur before the N-terminal SET domain, which catalyzes H3K4 methylation.

The majority (51%) of rrDLBCLs harbored a *TP53* mutation ($q = 2.25 \times 10^{-11}$; OR, 3.99). In contrast to *KMT2D*, mutations were predominately missense and affected the DNA-binding L1-sheet-helix domain (Figure 3B). We observed recurrent mutations affecting known *TP53* hotspots, including Arg175, Arg248, and Arg273, which either bind directly to DNA or coordinate DNA binding.[32] The Arg248 residue, which directly binds to the minor groove of DNA, was the only hotspot significantly enriched for mutations in rrDLBCL (q = 0.0807; OR, 3.29). In our untreated cohort, mutations in *TP53* and *KMT2D* were associated with inferior progression-free survival and overall survival (supplemental Figure 2), with *KMT2D* truncating mutations associated with inferior progression-free survival (supplemental Figure 3). This survival correlate was independent of other known prognostic factors, including the International Prognostic Index (IPI) and cell-of-orgin (COO) in a multivariate setting (supplemental Figure 4; supplemental Table 12).

The rrDLBCLs were also enriched for mutations affecting each of *CREBBP* (q = 0.0807; OR, 1.74), *NFKBIE* (q = 0.0232; OR, 2.78), and *FOXO1* (q = 0.087; OR, 2.33). The majority of *CREBBP* missense mutations affected the acetyltransferase domain (28/48 mutations, 58%) (Figure 3C), with the remainder predominantly causing truncation. Mutations in *FOXO1* could broadly be defined into 2 classes: those that disrupt the forkhead DNA-binding domain

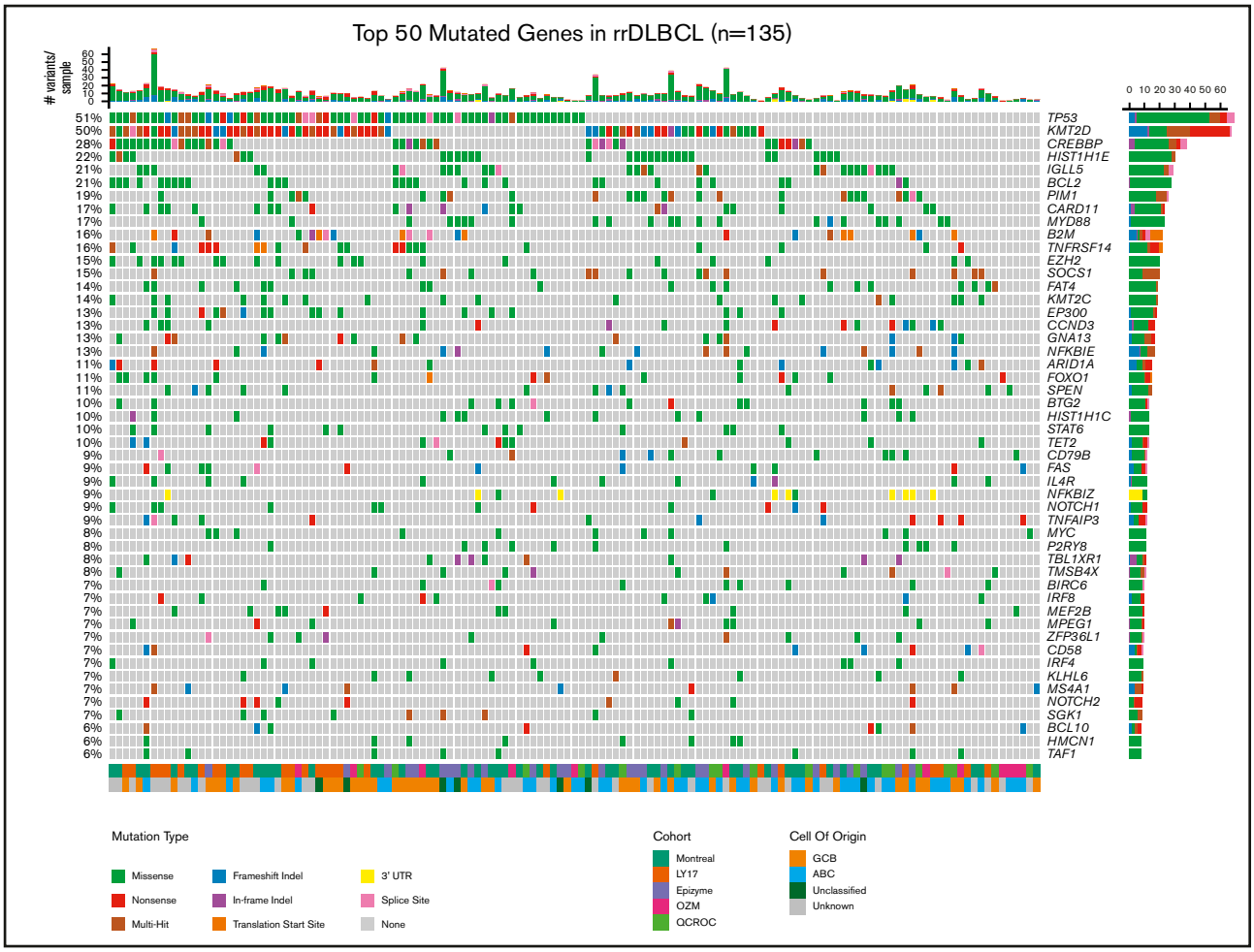

Figure 1. Mutation landscape of lymphoma-related genes in 135 rrDLBCL cases. Exonic mutations affecting the top 50 most recurrently mutated genes in our cohort of 135 rrDLBCL samples representing 5 different cohorts ("Methods"). The inferred effect of each mutation is indicated by color. Noncoding mutations are suppressed with the exception of *NFKBIZ*, which includes 3′ UTR mutations that have been previously described as driver mutations. The 2 covariate tracks on the bottom show COO information (where available) and the source cohort for each sample. Bar plots above and to the right of the plot indicate number of mutations per patient and number of patients with a mutation in that gene, respectively. Although the mutation landscape closely resembles untreated DLBCL, there are some notable differences. For example, approximately half of all rrDLBCLs harbored mutations in either *TP53* (51%) or the histone methyltransferase *KMT2D* (50%) with 31% of cases harboring mutations in both genes.

and those that disrupt *FOXO1* phosphorylation (Figure 3D). The latter include mutations-targeted Tyr24, adjacent residues, or the canonical start codon, which both affect the regulation of FOXO1 nuclear localization.[8] We also observed recurrent frameshift deletions affecting Tyr254 in *NFKBIE*, a negative regulator of NF-κB signaling (Figure 3E). Although mutations in *NFKBIE* were significantly enriched in rrDLBCL, the prevalence of mutations affecting the Tyr254 hotspot was not significantly higher in this cohort.

MS4A1 exhibited the strongest enrichment for mutations in rrDLBCL (q = 0.023; OR, 4.32). *MS4A1* encodes CD20, the B-lymphocyte antigen and target of rituximab and several other therapeutic mAbs. Although truncating mutations were observed across the length of *MS4A1*, a striking number of missense mutations were also observed (Figure 3F). None of these are predicted to directly affect residues comprising the rituximab epitope nor the epitopes of other mAbs. Instead, the recurrent missense variants were predicted to affect the transmembrane domains of the small loop, including 3 examples of a Tyr86 mutation (2 Tyr86Cys, 1 Tyr86His). Outside of rrDLBCL, mutations affecting this residue appear to be exceedingly rare as they were absent from the entire untreated DLBCL cohort and only appear in a single tumor in COSMIC.[33]

Recurrent clonal selection following rituximab-based therapy

To further explore genetic mechanisms that contribute to treatment resistance, we inferred the clonal structure and dynamics in the 57 patients with serially collected samples representing time points prior to and following rituximab-containing treatment regimens, including de novo DLBCL, tFL, and other B-cell lymphomas. For each set of samples, we inferred the CCF of each mutation detected in pretreatment tumor tissue biopsies and posttreatment plasma samples. We then compared individual CCFs between

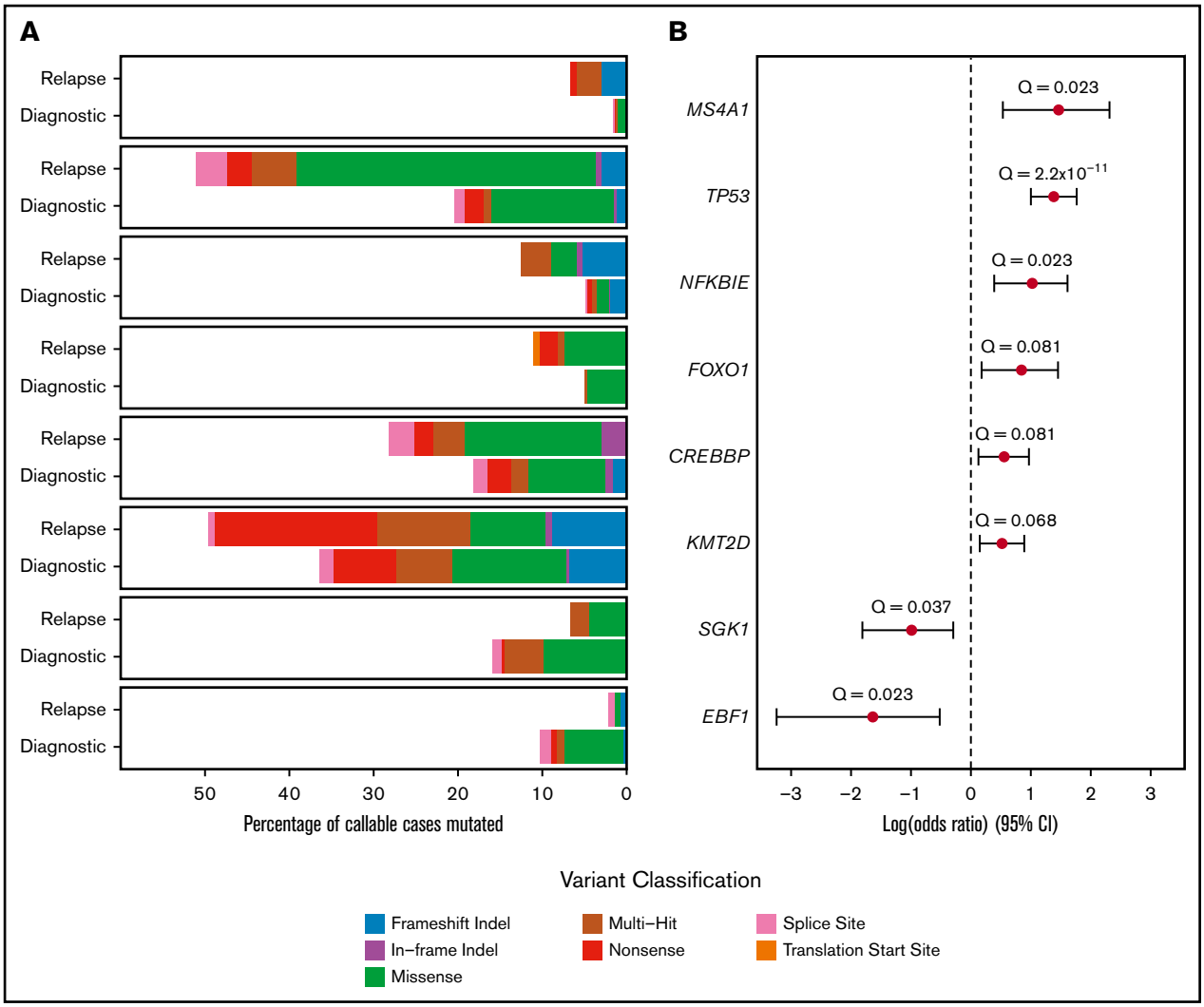

Figure 2. Differentially mutated genes between rrDLBCL and untreated DLBCL. (A) Mutation type and frequency of each differentially mutated gene in the untreated and rrDLBCL cohorts, using a significance threshold of 0.1 following false discovery rate correction. Untreated cases with insufficient coverage (not callable) in the gene of interest were not counted in the denominator for that gene (supplemental Methods). (B) Forest plot showing the odds ratio for all differentially mutated genes, as determined by the Fisher's exact test, for all differentially mutated genes (supplemental Table 6). CI, confidence interval.

paired samples and categorized mutations as enriched (clonal expansion), depleted (clonal regression), or stable at relapse within that tumor (Figure 4A). Figure 4B-I shows representative time series for mutations of interest. Overall, coding mutations affecting *TP53* (Figure 4B,D-I) and *KMT2D* (Figure 4D,F-G,I) tended to be stable following therapy, including all examples of *TP53* Arg248 mutations and *KMT2D* loss-of-function mutations (Figure 4D,F,I). We observed numerous examples showing clonal expansion of 1 *KMT2D* mutation and clonal depletion of a separate *KMT2D* mutation, suggesting a persistent selective advantage for *KMT2D* loss (Figure 4G). Mutations affecting *CREBBP* and *NFKBIE*, including *NFKBIE* Tyr254, were similarly stable prior to and following treatment in most patients. Taken together, mutations in these genes appear to generally represent a component of the founding clone.

In contrast to these genes, *MS4A1* mutations exhibited a consistent trend toward clonal expansion in patients following rituximab-containing therapy (Figure 4B-E). This includes several cases inferred to harbor multiple subclonal populations with distinct *MS4A1* mutations, with each exhibiting clonal expansion (Figure 4D). *MS4A1* mutations were consistently undetectable in diagnostic tissue and appear to result from consistent positive selection under the pressure of R-CHOP and other therapies. This trend along with their predominance in rrDLBCL relative to untreated DLBCLs indicates a role of these mutations in contributing to acquired treatment resistance during exposure to rituximab-containing therapy.

Mutations in *MS4A1* attenuate rituximab binding

We next explored the functional effects of *MS4A1* mutations and their potential role in promoting rituximab resistance. We transfected a $CD20^{-}$ cell line with WT or mutant CD20 constructs representing common *MS4A1* missense mutations observed in patients (Figure 5A). We showed that all 3 *MS4A1* mutants had significantly decreased binding of rituximab or other anti-CD20

Figure 3. Mutation patterns in genes enriched for mutations within the population of rrDLBCLs. Lollipop plots displaying the mutations discovered in the 6 genes (*KMT2D* [A], *TP53* [B], *CREBBP* [C], *FOXO1* [D], *NFKBIE* [E], *MS4A1* [F]) found to be significantly enriched for mutations at relapse compared with untreated DLBCL. Mutations in rrDLBCL are displayed above each gene, and mutations in the untreated cohort are displayed below each gene. The number of mutated cases and percentage of cases with mutations in that gene are shown beside each gene (red: relapse; blue: untreated). The size of a lollipop and vertical displacement represent the number of patients with nonsilent mutations observed at that position. Note that lollipops were scaled down in the untreated cohort, and thus, the size of a lollipop cannot be directly compared between the untreated and relapse cohorts. Relevant protein domains are displayed for genes with differing mutation patterns within these domains. There is a general enrichment for recurrent mutations in the untreated cohort, most pronounced in *KMT2D*. These are attributed to rare germline variants that we were unable to filter due to their absence in any database of common variants.

antibodies, including tositumomab (B1), ofatumumab, and obinutuzumab derivatives by flow cytometry, with 2 mutants (Y86C and L66R) showing a complete absence of binding (Figure 5B; supplemental Figure 5). Consistent with the other mutation tested, cells with ectopic expression of Tyr86Cys were not recognized by any of the anti-CD20 antibodies. In contrast, cells expressing Tyr86His were recognized by all 4 antibodies, albeit at a significantly reduced amount. Because this assay requires expression on the plasma membrane, we next explored whether the mutations affected the expression of CD20 within the cell using immunoblotting with a CD20 antibody that binds within the cytoplasmic domain. Consistent with the result from flow cytometry, an immunoblot of cell lysates showed reduced CD20 protein with the Y86H mutant and no visible expression with the other 2 mutants (Figure 5C). We separately performed CD20 staining on cell lines derived from tumors naturally harboring *MS4A1* mutations. Both Gly98Arg and Tyr86His cell lines were negative for CD20 staining by immunohistochemistry using L26, another mAb recognizing the C-terminal cytoplasmic region of CD20 (Figure 5D). Taken together, we conclude that *MS4A1* missense mutations can directly contribute to rituximab resistance by reducing CD20 expression and/or stability.

MS4A1-harboring subclones drive rapid treatment resistance

To further explore how multiple rounds of therapy can influence clonal structure in a *MS4A1*-mutant patient (PT255), we followed the progression of a patient with chemorefractory aggressive high-grade B-cell lymphoma using multiple complementary approaches (Figure 4B). We initially performed exome sequencing on 3 time points beginning with the untreated diagnostic tumor biopsy (diagnosis, D), followed by cfDNA collected after failure of both R-CHOP and subsequent high-dose chemotherapy (relapse 2, R2/P1) and a second cfDNA sample following additional rounds of chemotherapy including prednisone (relapse 3, R3/P5) (Figure 6A). We identified several distinct subclonal populations in these samples (Figure 6B) and selected mutations representative of each population: trunk (clonal), R2-associated (high prevalence at R2), and R3-associated (high prevalence at R3) for validation. We measured the variant allele frequency for these representative mutations in each time point and additional cfDNA samples and circulating tumor cells from blood collected between R2 and R3.

This analysis revealed a heterogenous clonal structure consisting of distinct subclones at each relapse (Figure 6C). Following R-CHOP

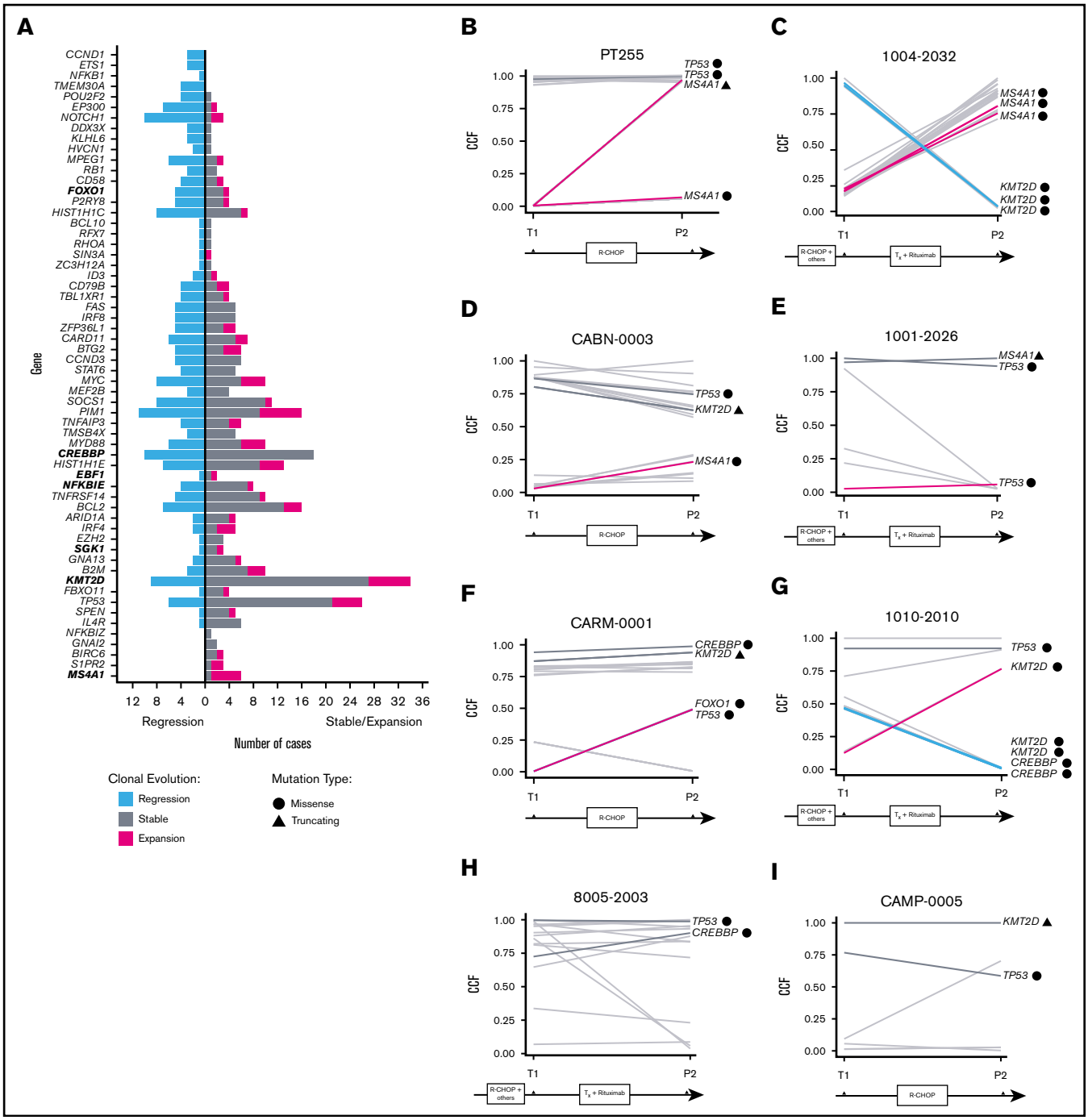

Figure 4. Clonal evolution patterns of regression and selection in rrDLBCL. (A) Number of cases with a mutation that regressed (blue), expanded (pink), or remained stable (gray) in a given gene following therapy. Time points are from a tumor biopsy before treatment (T1) and a plasma sample after treatment (P2). Genes in clusters that predominately undergo clonal expansion treatment are near the bottom, and genes in clusters depleted following treatment are near the top. (B-I) Clonal evolution plots for several patients following therapy, using a pretreatment tumor tissue biopsy and a posttreatment plasma sample. Each line represents a single coding mutation, and the relative CCF of each mutation before and after therapy is used to flag mutations that undergo clonal expansion (pink), depletion (blue), or remain stable (gray). The 8 genes differentially mutated are labeled and highlighted, and the mutation type is indicated by the adjacent symbol.

and high-dose chemotherapy (R2), we observed emergence of a population containing an *MS4A1* truncating mutation and a missense mutation within the kinase domain of *DDR2*, which has been described in lung cancer and may confer susceptibility to dasatinib.[34] This R2-associated subclone was undetectable at R3 and was replaced by a distinct population harboring a *MS4A1* missense mutation (Gly98Arg) and a truncating mutation affecting *NR3C1*, which encodes the glucocorticoid receptor and could

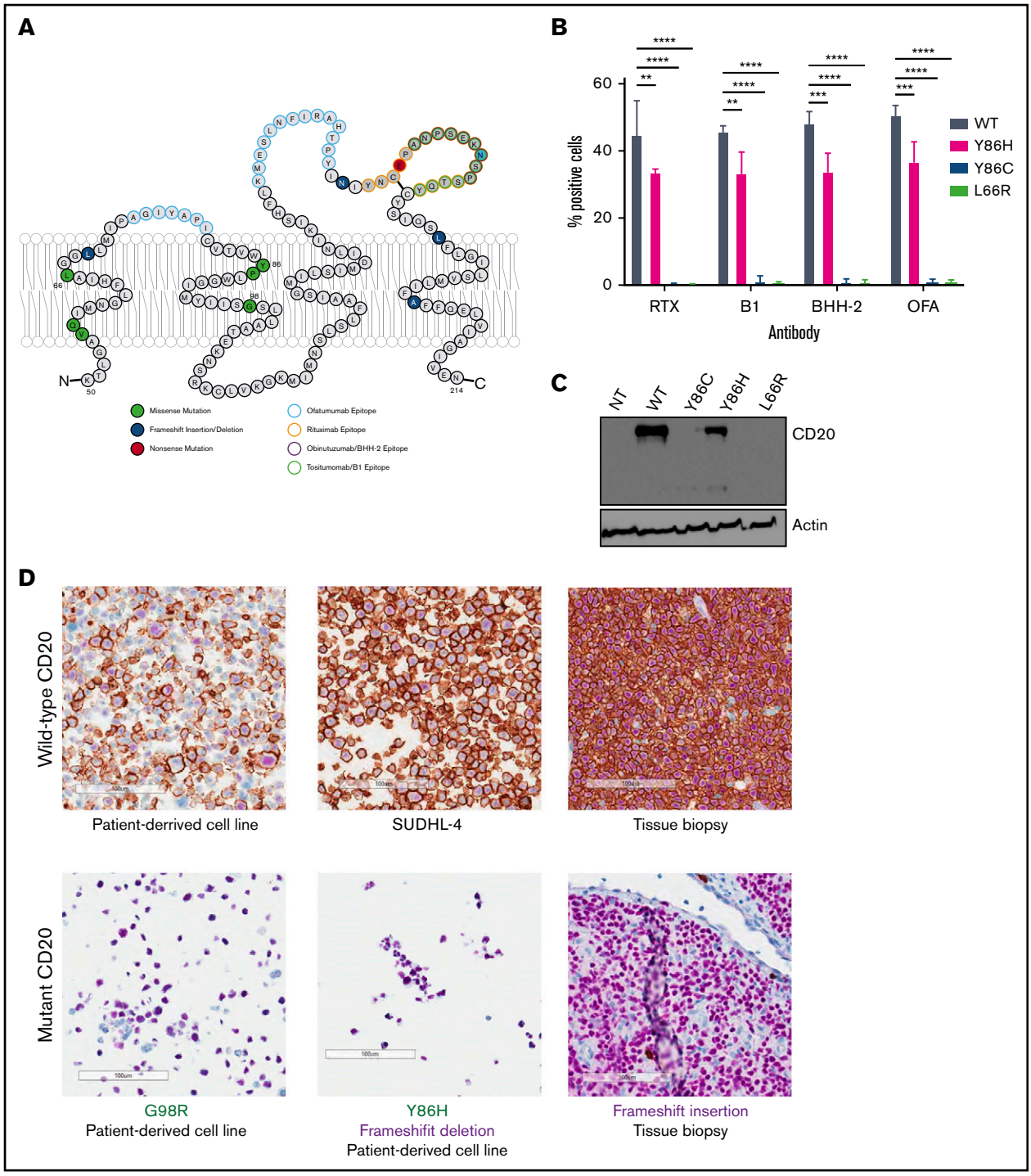

Figure 5. Distribution and functional impact of *MS4A1* mutations in rrDLBCL. (A) Topology of *MS4A1* transmembrane domains and extracellular loops, as annotated by Uniprot and elsewhere.[47] *MS4A1* mutations observed in the rrDLBCL cohort have been labeled, along with the predicted binding epitope of 4 different CD20 mAbs. (B) Comparison of antibody binding between CHO-S cells transfected with plasmids expressing either WT CD20 or 1 of 3 mutants (Tyr86His, Tyr86Cys, and Leu66Arg) for 4 different CD20 antibodies: rituximab (RTX), tositumomab (B1), obinutuzumab (BHH-2), or ofatumumab (OFA). The percent of positively stained cells was compared between mutants within each antibody (adjusted *P* values from 2-way analysis of variance of 3 replicates: **P* > .1, ***P* > .01, ****P* > .001, *****P* > .0001). See also supplemental Figure 5. (C) Representative western blot (of 2 independent experiments performed) showing CD20 expression of CHO-S cells transfected with WT or mutant CD20 (Y86H, Y86C, and L66R) and a nontransfected (NT) control. (D) Immunohistochemistry of CD20 in a cell line and tumor tissue biopsy harboring WT CD20 as well as 2 patient-derived cell lines harboring G98R (PT255), and Y86H along with a frameshift mutation, respectively. CD20 is stained red using the L26 CD20 antibody and B-cell nuclei were stained purple using a Pax5 antibody, visualized at ×20 original magnification.

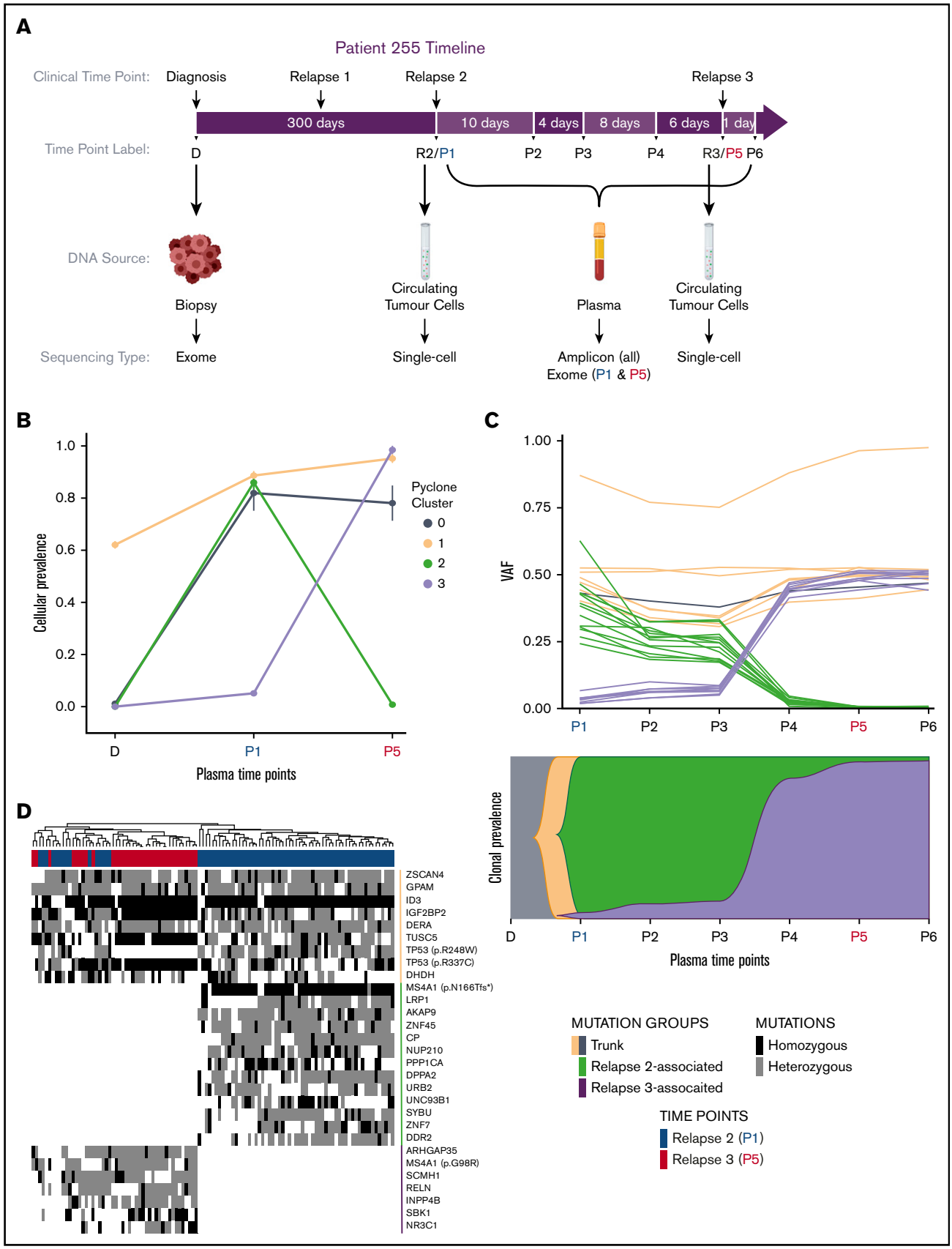

Figure 6.

contribute to resistance against steroids such as prednisone.[35] Although some mutations present in this later population were detectable at low levels following deep sequencing at R2, the extent of clonal expansion was striking given that <3 weeks elapsed between R2 and R3. In particular, this subclone exhibited rapid clonal expansion in the 8 days separating samples P3 and P4. Taken together, these data show that rapid changes in clonal structure can contribute to treatment resistance in DLBCL.

Given the emergence of subclones with different genetic features, we next sought to validate the clonal dynamics observed in R2 and R3 using single-cell sequencing. We determined mutation status and ploidy for the same set of mutations in a total of 74 isolated single cells from R2 and 35 isolated cells from R3. This confirmed that the R2-associated and R3-associated subclones exist in mutually exclusive subpopulations and confirmed the subpopulation at R2 representing the dominant clone found at R3 (Figure 6D). This also revealed genetic features that could not be inferred from bulk sequencing alone, such as a 17p deletion affecting *TP53* and *TUSC5* in the R3-associated clone and *MS4A1* loss of heterozygosity in the R2-associated clone. The *MS4A1* missense (R3-associated) and frameshift (R2-associated) mutations were detected in the majority of cells from each time point and thus were interpreted to represent early events in the foundation and development of these individual subclones. The vast majority of cells (> 99%) were negative for cell surface expression of CD20, consistent with each of these *MS4A1* mutations causing loss of CD20 expression. As rituximab can persist for weeks following treatment,[36] these *MS4A1* mutations likely provided the founder cells with a strong selective advantage, resulting in the independent emergence of multiple resistant subclones.

Discussion

By comparing the genetic landscapes of untreated and rrDLBCL, we highlight the potential role of 2 DLBCL-associated genes, *KMT2D* and *TP53*, as contributors to primary treatment resistance. Mutations affecting either gene were enriched in rrDLBCL and were typically clonal in matched pretreatment samples (Figure 4). *TP53* is known to be associated with inferior patient outcomes in DLBCL,[9,10] has been shown to be enriched for mutations in rrDLBCL,[7] and can contribute to resistance against chemotherapeutics, which induce DNA damage.[37,38] For instance, mutations affecting Arg248, a residue critical in DNA-binding that was enriched for mutations in our rrDLBCL cohort, can increase expression of cytochrome P450, which promotes resistance against a diverse range of chemotherapeutics in vitro and leads to inferior patient outcomes.[39] Given the high prevalence of *TP53* and *KMT2D* mutations in untreated DLBCL (20.7% and 36.9%, respectively), and their clonal prevalence and stability, mutations affecting these genes likely contribute to lymphomagenesis and primary refractory disease. Indeed, *KMT2D* mutations have been described as early drivers in DLBCL and FL[40] and contribute to increased cell survival and proliferation.[41] Although loss of H3K4me3 methylation results in transcriptional repression of numerous tumor suppressor genes, the contribution toward treatment resistance remains to be elucidated. *KMT2D* is commonly mutated in DLBCL overall, and these mutations may be enriched in the C3 genetic subgroup, which is associated with inferior prognosis within GCB-DLBCL.[26] Here, *KMT2D* mutations were associated with inferior prognosis in our untreated cohort regardless of COO or IPI (supplemental Figure 2). Together with genetic features such as double-hit/triple-hit, COO, and the DHITsig expression signature,[42] *KMT2D* and *TP53* mutations may facilitate the identification of high-risk patients for alternative treatments.

One barrier that has limited the genetic exploration of rrDLBCL is the lack of tissue biopsies, which are not routinely collected upon relapse. With sufficient levels of ctDNA, liquid biopsies have been shown to accurately reflect that mutational landscape of both the primary tumor and the distal sites.[19] Collection of posttreatment liquid biopsies is gaining adoption as it can noninvasively inform on treatment response[20,22,43] and, as demonstrated herein, affords the opportunity for serial sampling such that clonal dynamics can be inferred within the context of treatment resistance. As some patients in this study exhibited rapid changes in population structure (Figure 6), noninvasive methods will be required to allow prospective detection of resistance-associated mutations.

In this study, mutations in *MS4A1* recurrently exhibited clonal expansion following rituximab-based therapy (Figure 4). Single-cell analysis of a case harboring 2 mutually exclusive *MS4A1*-containing subclones revealed that these mutations were acquired after exposure to R-CHOP and became founder events for the multiple subclones that occurred at both relapses (Figure 6). Curiously, many *MS4A1* mutations were not predicted to truncate the protein, and these missense variants did not directly affect the rituximab binding epitope. Prior work utilizing Sanger sequencing and a smaller rrDLBCL cohort also found limited evidence for *MS4A1* mutations within the rituximab epitope,[44] leaving the phenomenon of reduced CD20 expression unexplained. We explored the influence of these mutations on anti-CD20 antibody interactions and found that common missense mutations attenuated mAb recognition (Figure 5B), largely as a result of reduced expression, with patient-derived cell lines harboring these mutations appearing on $CD20^{-}$ (Figure 5D). Although the underlying mechanism of CD20 loss stemming from these transmembrane domain missense mutations remains unresolved, the most likely explanation is that

Figure 6. Plasma and single-cell sequencing of multiple time points in a DLBCL patient (PT255). (A) Timeline of events for PT255. Clinical time point shows the timing of diagnosis (D) and relapses (R2, relapse 2; and R3, relapse 3) relative to blood sample collection (P1 to P6). Bulk tumor DNA was separately obtained from a biopsy at diagnosis, circulating tumor cells extracted at R2 and R3, and cfDNA extracted from plasma samples P1 to P6 after R2. Varying types of sequencing was performed on DNA from each time point, as summarized below. (B) Results from running PyClone on exome sequencing of DNA obtained from diagnosis, R2(P1,) and R3(P5). Clusters 0 and 1 contain trunk mutations seen at both P1 and P5; cluster 2 contains R2-specific mutations, and cluster 3 contains mutations that were subclonal at R2 and clonal at R3. (C) Amplicon sequencing of a subset of mutations found in the clusters in panel B from all 6 plasma time points reveal a more complete but similar evolution of the tumor as inferred from bulk sequence analysis in panel B. Below shows the suspected proportion of the tumor made up of each clone at individual time points. (D) Single-cell amplicon sequencing of circulating tumor cells taken at R2 and R3 revealed 2 distinct populations of cells containing mutations specific to each of R2 and R3. Genes are ordered by group and by frequency of mutation detected (top to bottom), suggesting a relative order of mutation acquisition.

they impair correct protein folding and subsequent stable expression, rather than simply destroying the antibody epitope(s), as 5 different mAbs were unable to detect expression, including one targeting the cytoplasmic domain in the C terminus. Given the low mutation frequency and low clonal prevalence of *MS4A1* mutations prior to therapy, we hypothesize that these mutations provide limited (if any) fitness advantage until the tumor is exposed to anti-CD20 antibodies. Furthermore, this suggests additional unidentified mechanisms by which tumor cells inhibit CD20 surface expression, possibly through other genetic or epigenetic mechanisms. These findings reinforce the necessity of evaluating tissue biopsies following relapse for CD20 expression in trials including immunotherapy targeting this protein. These CD20^{-} non-Hodgkin lymphoma cases are known to have poor outcomes with available therapies[45] and thus represent a population in need of alternative therapies.

In summary, we have identified 6 genes that are significantly enriched in rrDLBCL: *KMT2D*, *TP53*, *CREBBP*, *NFKBIE*, *FOXO1*, and *MS4A1*. The enrichment of *KMT2D* mutations in the rrDLBCL population and its association with inferior outcome suggests distinct biology or natural history of these DLBCLs, as *KMT2D* and *CREBBP* mutations are among the most common genetic feature of FL. One explanation for our observations is that a substantial proportion of de novo DLBCLs result from occult transformation from FL. Further evidence supporting this possibility has recently been gleaned through the genetic analysis of DLBCLs with *MYC* and *BCL2* translocations.[46] In contrast to these early mutations, *MS4A1* mutations are rare in untreated DLBCL and were generally undetectable prior to therapy. Our data indicate that these mutations directly contribute to rituximab resistance, resulting in rapid clonal selection and expansion in the presence of rituximab-containing therapy. Furthermore, our single-cell data highlight the significant clonal heterogeneity of rrDLBCL, and the contribution of *MS4A1* mutations toward rapid treatment resistance. The recurrent loss of CD20 expression in the rrDLBCL population may have profound implications given the widespread use of rituximab and the ongoing targeting of CD20 with additional mAbs and more modern forms of immunotherapy.

Acknowledgments

The authors acknowledge the support of the patients and their families, who have consented to participate in lymphoma tissue banking within the Banque de Cellules Leucémiques du Québec at the Jewish General Hospital (JGH). The authors thank the Jewish General Hospital Foundation and the Cole Foundation for supporting the Lymphoma Cell Bank at the JGH.

This work was supported by Terry Fox New Investigator Award 1021 and Program Project grants 1043 and 1061. R.D.M. holds a Canadian Institutes of Health Research (CIHR) New Investigator Award and a Scholar of Michael Smith Foundation for Health Research. The authors gratefully acknowledge funding support from the Terry Fox Research Institute (J.M.C.), Genome Canada (J.M.C. and C.S.), Genome British Columbia (J.M.C.), CIHR (J.M.C., R.D.M., and N.A.J.), and the British Columbia Cancer Foundation (J.M.C. and R.D.M.). N.A.J. is also supported by funds from Canadian Cancer Society Research Institute (705478).

Authorship

Contribution: R.D.M., D.W.S., and N.A.J. conceptualized the study; R.D.M. provided the methodology; C.K.R. provided the software; C.K.R., S.E.A., M.A., A.J., K.M.C., N.T., L.K.H., K.L.S.C., and M.S.C. provided the formal analysis; C.K.R., S.E.A., M.A., R.N.R., K.M.C., and A.J. led the investigation; S.E.A., M.A., M. Cheung, N.M., S.D., J.D., R.N.R., K.B., S.Y., M.J., L.S., J.K., M. Crump, M.S.C., K.M., S.A., and N.A.J. provided the resources; C.K.R., M.A., and N.A.J. curated the data; C.K.R., S.E.A., M.A., R.D.M., D.W.S., and N.A.J. contributed to writing of the original draft:; C.K.R., S.E.A., and R.D.M. provided the visualization; S.E.A. and C.K.R. contributed to the writing, review, and editing; R.D.M., N.A.J., and D.W.S. provided supervision; and R.D.M., D.W.S., N.A.J., J.M.C., M.A.M., and C.S. contributed to acquiring funding.

Conflict-of-interest disclosure: S.D. and N.M. are employees of Epizyme. M.J. provides consultancy/advisory for Kite/Gilead and Novartis. M.C. provides a consultancy/advisory role for Kite/Gilead, Roche, and Servier. J.K. provides a consultancy/advisory role for Abbvie Canadian Cancer Society Research Institute, Amgen, AstraZeneca, BMS, Celgene, Gilead, Janssen, Karyopharm, Merck, Novartis, Roche, and Seattle Genetics. The remaining authors declare no competing financial interests.

ORCID profiles: C.K.R., 0000-0001-6306-9361; S.E.A., 0000-0002-5341-7868; K.M.C., 0000-0002-1309-4873; K.L.S.C., 0000-0001-6200-4945; L.K.H., 0000-0002-6413-6586; M.J., 0000-0002-7789-1257; M.A.M., 0000-0001-7146-7175; M.S.C., 0000-0003-2077-089X; R.D.M., 0000-0003-2932-7800.

Correspondence: Ryan D. Morin, Department of Molecular Biology and Biochemistry, Simon Fraser University, 8888 University Dr, Burnaby, BC V5A 1S6, Canada; e-mail: rdmorin@sfu.ca.

References

1. Maurer MJ, Ghesquières H, Jais J-P, et al. Event-free survival at 24 months is a robust end point for disease-related outcome in diffuse large B-cell lymphoma treated with immunochemotherapy. *J Clin Oncol*. 2014;32(10):1066-1073.
2. Mounier N, Briere J, Gisselbrecht C, et al. Rituximab plus CHOP (R-CHOP) overcomes bcl-2–associated resistance to chemotherapy in elderly patients with diffuse large B-cell lymphoma (DLBCL). *Blood*. 2003;101(11):4279-4284.
3. Rovira J, Valera A, Colomo L, et al. Prognosis of patients with diffuse large B cell lymphoma not reaching complete response or relapsing after frontline chemotherapy or immunochemotherapy. *Ann Hematol*. 2015;94(5):803-812.
4. Crump M, Neelapu SS, Farooq U, et al. Outcomes in refractory diffuse large B-cell lymphoma: results from the international SCHOLAR-1 study [published correction appears in *Blood*. 2018;131(5):587-588]. *Blood*. 2017;130(16):1800-1808.
5. Nijland M, Seitz A, Terpstra M, et al. Mutational evolution in relapsed diffuse large B-cell lymphoma. *Cancers (Basel)*. 2018;10(11):459.

6. Morin RD, Assouline S, Alcaide M, et al. Genetic landscapes of relapsed and refractory diffuse large B-cell lymphomas. *Clin Cancer Res*. 2016;22(9):2290-2300.
7. Mareschal S, Dubois S, Viailly P-J, et al. Whole exome sequencing of relapsed/refractory patients expands the repertoire of somatic mutations in diffuse large B-cell lymphoma. *Genes Chromosomes Cancer*. 2016;55(3):251-267.
8. Trinh DL, Scott DW, Morin RD, et al. Analysis of FOXO1 mutations in diffuse large B-cell lymphoma. *Blood*. 2013;121(18):3666-3674.
9. Xu-Monette ZY, Wu L, Visco C, et al. Mutational profile and prognostic significance of TP53 in diffuse large B-cell lymphoma patients treated with R-CHOP: report from an International DLBCL Rituximab-CHOP Consortium Program Study. *Blood*. 2012;120(19):3986-3996.
10. Zenz T, Kreuz M, Fuge M, et al; German High-Grade Non-Hodgkin Lymphoma Study Group (DSHNHL). TP53 mutation and survival in aggressive B cell lymphoma. *Int J Cancer*. 2017;141(7):1381-1388.
11. Greenawalt DM, Liang WS, Saif S, et al. Comparative analysis of primary versus relapse/refractory DLBCL identifies shifts in mutation spectrum. *Oncotarget*. 2017;8(59):99237-99244.
12. Melchardt T, Hufnagl C, Weinstock DM, et al. Clonal evolution in relapsed and refractory diffuse large B-cell lymphoma is characterized by high dynamics of subclones. *Oncotarget*. 2016;7(32):51494-51502.
13. Chan KCA, Jiang P, Zheng YWL, et al. Cancer genome scanning in plasma: detection of tumor-associated copy number aberrations, single-nucleotide variants, and tumoral heterogeneity by massively parallel sequencing. *Clin Chem*. 2013;59(1):211-224.
14. Cheng H, Liu C, Jiang J, et al. Analysis of ctDNA to predict prognosis and monitor treatment responses in metastatic pancreatic cancer patients. *Int J Cancer*. 2017;140(10):2344-2350.
15. Kurtz DM, Scherer F, Jin MC, et al. Circulating tumor DNA measurements as early outcome predictors in diffuse large B-cell lymphoma. *J Clin Oncol*. 2018;36(28):2845-2853.
16. Thierry AR, El Messaoudi S, Gahan PB, Anker P, Stroun M. Origins, structures, and functions of circulating DNA in oncology. *Cancer Metastasis Rev*. 2016;35(3):347-376.
17. Wan JCM, Massie C, Garcia-Corbacho J, et al. Liquid biopsies come of age: towards implementation of circulating tumour DNA. *Nat Rev Cancer*. 2017;17(4):223-238.
18. Newman AM, Bratman SV, To J, et al. An ultrasensitive method for quantitating circulating tumor DNA with broad patient coverage. *Nat Med*. 2014;20(5):548-554.
19. Rossi D, Diop F, Spaccarotella E, et al. Diffuse large B-cell lymphoma genotyping on the liquid biopsy. *Blood*. 2017;129(14):1947-1957.
20. Chabon JJ, Simmons AD, Lovejoy AF, et al. Circulating tumour DNA profiling reveals heterogeneity of EGFR inhibitor resistance mechanisms in lung cancer patients [published correction appears in *Nat Commun*. 2016;7:13513]. *Nat Commun*. 2016;7(1):11815.
21. Murtaza M, Dawson S-J, Pogrebniak K, et al. Multifocal clonal evolution characterized using circulating tumour DNA in a case of metastatic breast cancer. *Nat Commun*. 2015;6(1):8760.
22. Assouline SE, Nielsen TH, Yu S, et al. Phase 2 study of panobinostat with or without rituximab in relapsed diffuse large B-cell lymphoma. *Blood*. 2016;128(2):185-194.
23. Kim S, Scheffler K, Halpern AL, et al. Strelka2: fast and accurate calling of germline and somatic variants. *Nat Methods*. 2018;15(8):591-594.
24. Reddy A, Zhang J, Davis NS, et al. Genetic and functional drivers of diffuse large B cell lymphoma. *Cell*. 2017;171(2):481-494.e15.
25. Schmitz R, Wright GW, Huang DW, et al. Genetics and pathogenesis of diffuse large B-cell lymphoma. *N Engl J Med*. 2018;378(15):1396-1407.
26. Chapuy B, Stewart C, Dunford AJ, et al. Molecular subtypes of diffuse large B cell lymphoma are associated with distinct pathogenic mechanisms and outcomes [published corrections appears in Nat Med. 2018;24(8):1292; Nat Med. 2018;24(8):1290-1291]. *Nat Med*. 2018;24(5):679-690.
27. Arthur SE, Jiang A, Grande BM, et al. Genome-wide discovery of somatic regulatory variants in diffuse large B-cell lymphoma. *Nat Commun*. 2018;9(1):4001.
28. Lacy SE, Barrans SL, Beer PA, et al. Targeted sequencing in DLBCL, molecular subtypes, and outcomes: a Haematological Malignancy Research Network report. *Blood*. 2020;135(20):1759-1771.
29. Wright GW, Huang DW, Phelan JD, et al. A probabilistic classification tool for genetic subtypes of diffuse large B cell lymphoma with therapeutic implications. *Cancer Cell*. 2020;37(4):551-568.e14.
30. Cleary KLS, Chan HTC, James S, Glennie MJ, Cragg MS. Antibody distance from the cell membrane regulates antibody effector mechanisms. *J Immunol Baltim Md 1950*. 2017;198(10):3999-4011.
31. Morin RD, Mendez-Lago M, Mungall AJ, et al. Frequent mutation of histone-modifying genes in non-Hodgkin lymphoma. *Nature*. 2011;476(7360):298-303.
32. Baugh EH, Ke H, Levine AJ, Bonneau RA, Chan CS. Why are there hotspot mutations in the TP53 gene in human cancers? *Cell Death Differ*. 2018;25(1):154-160.
33. Tate JG, Bamford S, Jubb HC, et al. COSMIC: the Catalogue Of Somatic Mutations In Cancer. *Nucleic Acids Res*. 2019;47(D1):D941-D947.
34. Xu C, Buczkowski KA, Zhang Y, et al. NSCLC driven by DDR2 mutation is sensitive to dasatinib and JQ1 combination therapy. *Mol Cancer Ther*. 2015;14(10):2382-2389.
35. Haowen X, Ding Y, Gao Y, et al. Haploinsufficiency for NR3C1 drives glucocorticoid resistance by inactivation the PI3K/AKT/GSK3β/Bim pathway in adult acute lymphoblastic leukemia [abstract]. *Blood*. 2018;132(suppl 1).Abstract 1328.

36. Regazzi MB, Iacona I, Avanzini MA, et al. Pharmacokinetic behavior of rituximab: a study of different schedules of administration for heterogeneous clinical settings. *Ther Drug Monit*. 2005;27(6):785-792.

37. Sun Y, Xia P, Zhang H, Liu B, Shi Y. P53 is required for doxorubicin-induced apoptosis via the TGF-beta signaling pathway in osteosarcoma-derived cells. *Am J Cancer Res*. 2015;6(1):114-125.

38. Ungerleider NA, Rao SG, Shahbandi A, et al. Breast cancer survival predicted by TP53 mutation status differs markedly depending on treatment. *Breast Cancer Res*. 2018;20(1):115.

39. Xu J, Wang J, Hu Y, et al. Unequal prognostic potentials of p53 gain-of-function mutations in human cancers associate with drug-metabolizing activity. *Cell Death Dis*. 2014;5(3):e1108.

40. Zhang J, Dominguez-Sola D, Hussein S, et al. Disruption of KMT2D perturbs germinal center B cell development and promotes lymphomagenesis. *Nat Med*. 2015;21(10):1190-1198.

41. Ortega-Molina A, Boss IW, Canela A, et al. The histone lysine methyltransferase KMT2D sustains a gene expression program that represses B cell lymphoma development. *Nat Med*. 2015;21(10):1199-1208.

42. Ennishi D, Jiang A, Boyle M, et al. Double-hit gene expression signature defines a distinct subgroup of germinal center B-cell-like diffuse large B-cell lymphoma. *J Clin Oncol*. 2019;37(3):190-201.

43. Roschewski M, Staudt LM, Wilson WH. Dynamic monitoring of circulating tumor DNA in non-Hodgkin lymphoma. *Blood*. 2016;127(25):3127-3132.

44. Johnson NA, Leach S, Woolcock B, et al. CD20 mutations involving the rituximab epitope are rare in diffuse large B-cell lymphomas and are not a significant cause of R-CHOP failure. *Haematologica*. 2009;94(3):423-427.

45. Qunaj L, Castillo JJ, Olszewski AJ. Survival of patients with CD20-negative variants of large B-cell lymphoma: an analysis of the National Cancer Data Base. *Leuk Lymphoma*. 2018;59(6):1375-1383.

46. Cucco F, Barrans S, Sha C, et al. Distinct genetic changes reveal evolutionary history and heterogeneous molecular grade of DLBCL with MYC/BCL2 double-hit. *Leukemia*. 2020;34(5):1329-1341.

47. Teeling JL, Mackus WJM, Wiegman LJJM, et al. The biological activity of human CD20 monoclonal antibodies is linked to unique epitopes on CD20. *J Immunol*. 2006;177(1):362-371.